Reel-to-Reel Fabrication of Smart Sensing Threads

Ege Ozgul
Electrical Engineering Department
Tufts University
Medford, United States
ege.ozgul@Tufts.edu

Wenxin Zeng
Electrical Engineering Department
Tufts University
Medford, United States
wenxin.zeng@tufts.edu

Sameer Sonkusale
Electrical Engineering Department
Tufts University
Medford, United States
sameer.sonkusale@Tufts.edu

***Abstract*—With favorable properties of stretchability, stitchability, and potential to wove into a fabric, thread-based sensors have gained a large amount of interests for wearable devices and the Internet of Bodies (IoB) applications. To facilitate the IoB, an easy and reliable way to fabricate these thread-based sensors with good performance and consistency is the key. In this paper, we propose an automatic strain-sensing thread coating system, that can fabricate thread-based strain sensors with controlled parameters. The proposed system is not only capable of fabricating the strain sensor, but also characterizing the sensitivity and consistency of the fabricated thread. With the system, a sample thread with a sensitivity of 32.64 KΩ/N is prepared. Compared with hand-coated thread, the machine-fabricated thread shows much better sensitivity and consistency. The prepared strain-sensor is made into a respiration sensor patch and a limb motion patch to demonstrate the application.**

I. Introduction

With the increasing demand for wearable sensors for the Internet of Bodies (IoB), research effort has been drawn to the development and fabrication of strain sensors with low-cost and simple processes. Unlike conventional strain sensors that consist of rigid and fragile piezoresistors, wearable devices require flexibility and stretchability to be practical in actual applications [1]. As a result, sensors in various formats, such as textiles, nanofiber, or hydrogel, have been studied to monitor the motion of the human body [2]–[8]. Having a one-dimensional geometry, the thread is a suitable material to achieve strain sensing with low cost, simple structure, and easy fabrication [9]. Moreover, the intrinsic properties of the thread enable it to be woven onto a fabric easily, greatly broadening the capabilities of a wearable device [10].

Thread-based strain sensors have intensively studies for various applications [11]–[21]. In previous works, thread-based strain sensors have been demonstrated to detect the weight distribution of foot [22], head motion [23], and touching [24]. These proposed wearable devices were achieved by a stretchable strain-sensing thread that is lightweight, easy to fabricate, and sensitive. The thread strain sensor was made by manually coating carbon ink on the surface of elastic threads [25]. After the carbon ink dried, the threads were coated with PDMS for protection. The carbon forms conductive particles on the surface of the thread. When stretched, the distances between particles increase as the elastic thread expands. As a result, the resistance thread increases. Once the thread is relaxed, the particles move back to the original position and the resistance changes back. The initial resistivity and sensitivity of the strain-sensing thread are determined by the volume of the carbon ink coated on the thread. However, the manual coating process introduced large variations in the fabricated threads. To achieve consistent carbon thread fabrication, a reel-to-reel thread manufacturing system was designed [22]. The system was able to produce strain-sensing thread with a fixed resistivity, but one could not control the coating thickness, nor monitor the resistivity during the fabrication process.

In this work, we propose an improved strain-sensing thread fabrication system that can achieve more flexibility on the parameters of the threads. Thread fabrication, monitoring, and testing are all integrated into one system. The threads fabricated in one run are much more consistent than the hand-coated counterpart. The sensitivity of the fabricated sample thread is from 32.64 KΩ/N. The linear regression of the measured data shows an R-Square value of 0.9595. To demonstrate the application of the strain-sensing thread, a respiration sensor and limb motion sensor are shown. The respiration sensor monitors the chest expansion and contraction caused by breathing, and is possible to detect volume changes in the lung with proper calibration. The limb motion sensor can monitor the range of motion of arms and legs.

II. Design

The smart thread factory system is composed of multiple components that work together to allow the user to manufacture consistent high-quality threads with desired parameters. The conceptual design of the whole system is illustrated in Fig. 1. In this part of the paper, each of these parts is explained in more depth, including the ink cartridge, the drying chamber, the tension regulator, the microcontroller and the user interface.

A. Ink Cartridge

The cartridge is a crucial element responsible for the application of conductive ink onto the thread. It features two gates on either side and three finger-like structures Within the cartridge, as illustrated in yellow in Fig. 2(a). The finger-like structures exert opposing pressure on the thread, enhancing the absorption of the carbon ink. Initially, the gates are kept open to facilitate the installation of the thread, denoted in red, as shown in Fig. 2(b). Subsequently, the gates are sealed,

Thanks to the Tufts NanoLab Laboratory.

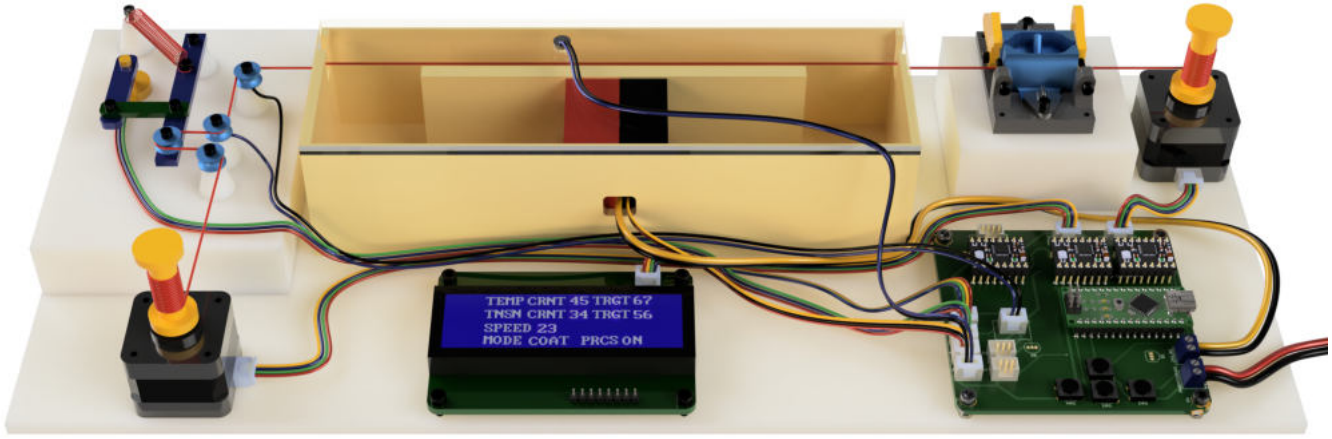

Fig. 1. Schematic of the smart thread coating factory.

encapsulating the cartridge, as in Fig. 2(c), followed by the injection of conductive ink from the top via a syringe. The yellow gates on the cartridge are equipped with V-shaped notches that come in contact with the thread, controlling the residual ink as the thread exits the cartridge. The user can manipulate the notch's position by adjusting the bolts on the cartridge's side, thereby altering the gate's position when closed. Tightening the bolts increases the notch's size, allowing a greater quantity of ink to remain on the thread as it departs from the cartridge. Conversely, loosening the thread narrows the gates and reduces the notch's size, resulting in a diminished ink volume on the thread.

Upon commencement of the coating procedure, a stepper motor draws the thread in and out of the cartridge. Over time, dry ink will accumulate in the cartridge and eventually prevent the cartridge from working. To address this issue, the cartridge is designed for single use and is detachable from the system, allowing for effortless removal and replacement. It can be 3D printed using PLA, making it highly convenient to fabricate and replace, which is more practical and economical than cleaning a used one.

B. Drying Chamber

Following the ink cartridge, a drying chamber is designed to facilitate the ink's drying process. As depicted in Fig. 3, the chamber allows the thread to move through and directs hot air onto the coated thread. Within this heated enclosure, a fan and a resistive heater work in tandem to circulate the warm air. This enclosed design ensures that the heated air remains confined, allowing the resistive heater to maintain the temperature of the same air without expending additional power. Additionally, a temperature sensor is positioned close to the path of the thread. A microcontroller continuously monitors the air temperature in the chamber. The resistive heater is activated when the air temperature is below the desired temperature and is deactivated when the air temperature is above the target temperature. The fan operates non-stop, ensuring a constant airflow, which allows the heater to immediately change the air temperature.

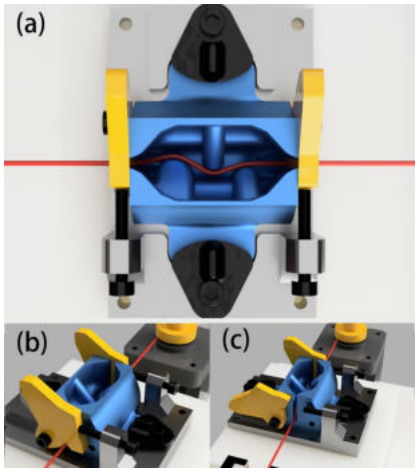

Fig. 2. Cartridge (a) top view, (b) side view with gate open, and (c) side view with gate closed.

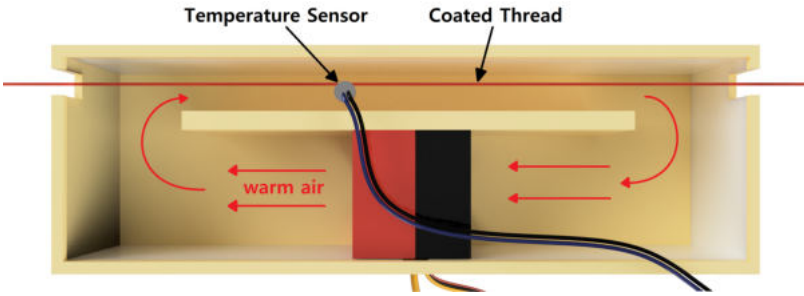

Fig. 3. Top view of the schematic of the drying Chamber.

C. Thread Tension Regulator

The system utilizes two stepper motors to transfer the raw thread from the input spool to the output spool, as shown in the top-right and bottom-left corners in Fig. 1, by rotating the spools independently. During the coating process, a consistent tension of the thread is key to producing a uniform thread that has an identical tension vs. resistance correlation along

the thread. A thread tension regulator is designed to monitor and adjust the tension of the thread in real-time.

A PID feedback controller monitors and regulates the thread tension, and keeps it at the target value. The target tension value can be set using the user interface on the device. The PID algorithm (see Fig. 4) is implemented in the micro-controller which constantly measures the tension on the thread, and adjusts the speed of the the output spool based on the error between the current tension and the target. More information about the custom tension sensor is discussed in the following subsection.

The following PID model is implemented in the firmware of the device, where e(t) is the tension error variable, which equals the target tension minus current tension. Variable u(t) represents the amount of rotation that the stepper motor will cover at the current system loop.

$$u(t) = K_p e(t) + K_i \int e(t)dt + K_d \frac{de(t)}{dt}$$

k_d, k_i, and k_p are the PID constants that are used in the feedback system. The values are computed experimentally and provided below.

$$k_d = 2.651f * 10^{(-7)}$$
$$k_i = 1.238f * 10^{(-4)}$$
$$k_p = 1.519f * 10^{(2)}$$

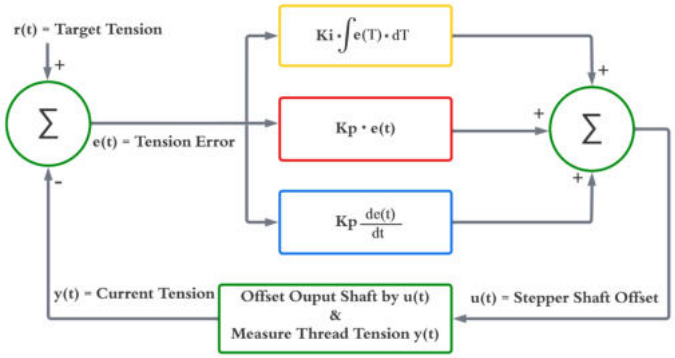

Fig. 4. Feedback control algorithm.

1) Tension Sensor: The tension sensor (see in Fig. 5) is the main component of the tension regulator which allows the feedback control system to monitor the tension of the thread at high frequency and manipulate the tension by changing the speed of the output spool. The red spring shown in Fig. 5 applies counter tension to the thread via the blue lever, so that he angle of the blue lever is directly correlated with the tension on the thread. When the thread is at high tension, the blue lever rotates counterclockwise; and when there is less tension, it rotates clockwise. A potentiometer (denoted as Pot) is used for measuring the angle of this lever, which produces an analog signal between 0 to 5 Volts. Then a 10-bit ADC is used to convert this voltage to a digital integer value between 0 and 1023.

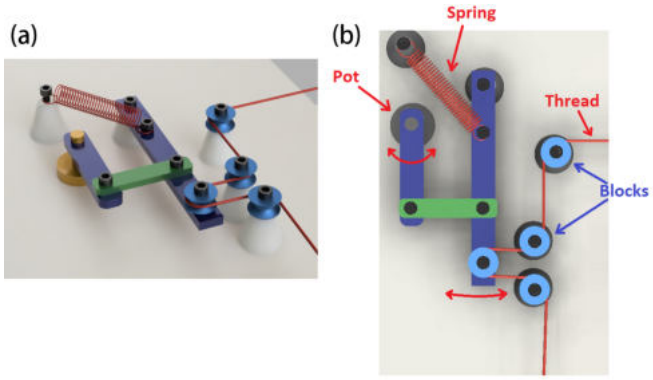

Fig. 5. (a) Schematic of the tension sensor, (b) Top view of the tension sensor (Pot stands for potentiometer).

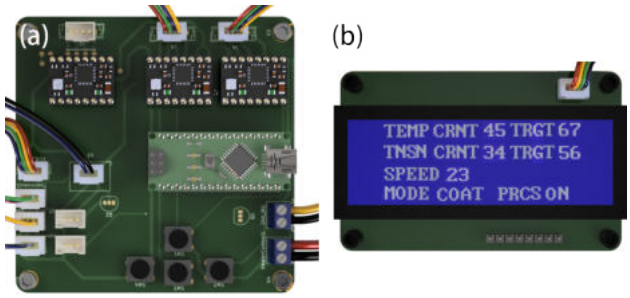

Fig. 6. (a) Motherboard, (b) LCD Panel

2) User Interface: The user interface (See Fig. 6) consists of an LCD screen and 4 push buttons that are placed on the motherboard. The LCD screen displays the parameters listed below.

- Target temperature Current measured temperature
- Target thread tension Current thread tension
- Spool speed
- Process State: On, Off
- Process Mode: Coat, Consistency Test, Stretch Test

4 push buttons placed on the motherboard (see Fig. 6) allow the user to adjust the coating parameters in the list above. Up and down buttons allow selecting the parameter to be adjusted. Left and right buttons allow the user to increase or decrease the parameters. Process state is a boolean parameter that allows the user to start and stop the process mode selected by the user. There are three process modes. "Coat" mode is the main coating process. "Consistency Test" mode is used for the conductivity test of the entire coated thread. By constantly spinning the input and output spools while regulating the tension, the system can measure the resistance between the two metal blocks connected to the microcontroller (See Fig. 5). "Stretch test" precisely stretches and releases the coated thread in cycles, which is used for characterizing the coated threads. The consistency and stretch testing modes are utilized to automate the data collection that is presented in the following part. A photo of the whole coating system is shown in Fig. 7.

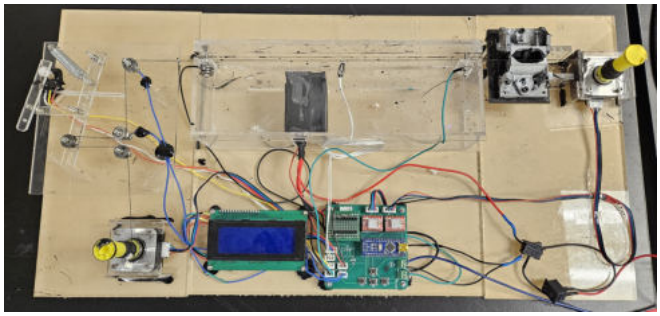

Fig. 7. Photo of the actual device.

III. Thread Analysis and Characterization

To characterize the fabricated thread, it is analyzed under an optical microscope and SEM, and then tested for its resistance and consistency at different conditions. Fig. 8(a) shows the coated thread in its natural state under the optical microscope. In this case, the carbon particles are tightly connected together, therefore the electrical resistance is relatively lower (112 KΩ/cm). Fig. 8(b) and (c) also show the SEM images of the thread in the natural state. It can be seen that multiple carbon particles overlap with each other to create a continuous connection. Fig. 8(d) shows the stretched thread from the optical microscope. In this case, the carbon particles are separated due to the elongation of the thread. As a result, the carbon coating has a higher resistance (251 KΩ/cm). Fig. 8(e) and (f) show the SEM images of the stretched thread. At this state, the carbon particles are torn apart and the thread area without carbon covering is visible. The SEM images of the coated thread cross-section are shown in Fig. 8(g) and (h).

The coating device is capable of performing tests on the coated threads by using the existing stepper motors and sensors. There are two test processes programmed into the device's microcontroller: Consistency Test and Stretch Test.

A. Characterization of the Coated Threads

For characterizing the threads, "Stretch Test" process is selected on the user interface and executed. During the process, only the stepper motor for the output spool rotates to stretch and release the coated thread. For this test, the microcontroller is programmed to stretch and release the thread for a total of 1000 times, While recording the tension and the resistance of the thread. The collected data is continuously sent to a computer via a serial interface.

Fig. 9(a) shows the measured and linear regression data between the tension and the resistance of the sample thread that is coated automatically by the system. The fabricated sample thread has a sensitivity of 32.64 KΩ/N. The R-Square value of the fitting is 0.9595. Fig. 9(c) displays the collected and linear regression data of the thread that is coated by hand. For the hand-coated thread, the sensitivity is 17.24 KΩ/N and the R-Square value of the fitting is 0.5494. The machine-coated thread has much higher sensitivity and is more consistent during the stretching. Resistance vs. Cycle graphs are plotted in Fig. 9(e) and (f). The minimum and maximum resistance values at each cycle stay consistent for 1000 cycles, which indicates the reliable durability of the fabricated thread.

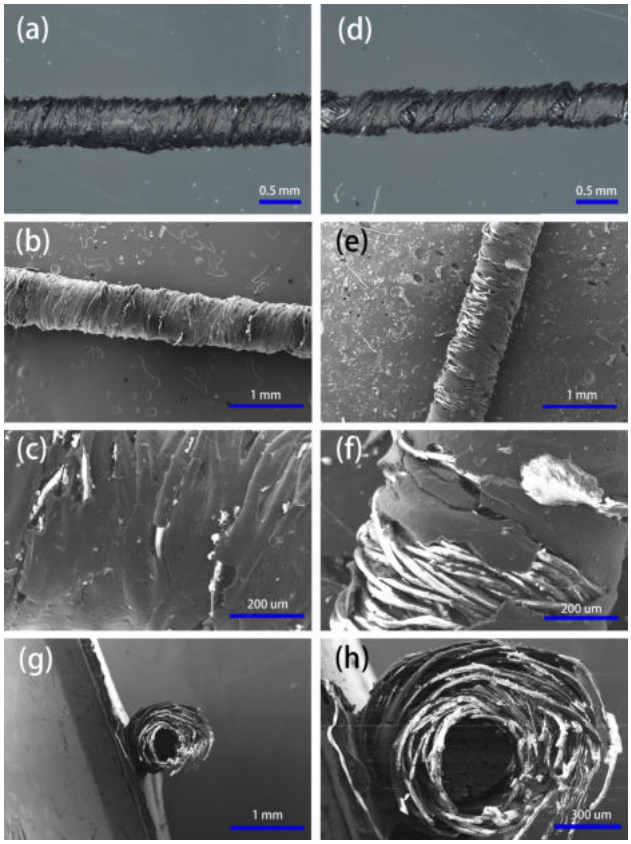

Fig. 8. Strain sensor at relaxed state under (a) optical microscope and (b), (c) under SEM. Strain sensor at stretched state under (d) optical microscope and (e), (f) under SEM. (g), (h) Cross-section image under SEM.

B. Resistance Consistency Test

The coating device is also capable of performing resistance consistency tests. For this test, the device transfers all the coated threads from the input spool to the output spool by using the stepper motors. While moving the thread, the resistance between the metal blocks is measured continuously. These two metal blocks are connected to the ADC of the microcontroller, which measures the resistance between the blocks and sends the data to a computer using the serial interface. Fig. 8(b) shows the consistency data of the thread that is coated automatically by the device, and Fig. 8(d) shows the data of a hand-coated thread. It can be seen that the machine-coated thread is much more consistent and precise compared to the hand-coated one.

C. Filtering

Even though the automatic coating process of the device enhances the quality of the thread, there is still a significant amount of noise in the data collected from the measurement. To further reduce the noise in the data, moving average filtering algorithms are utilized with window sizes of 5, 14, and 27 data points. As shown in Fig. 10, with a larger window

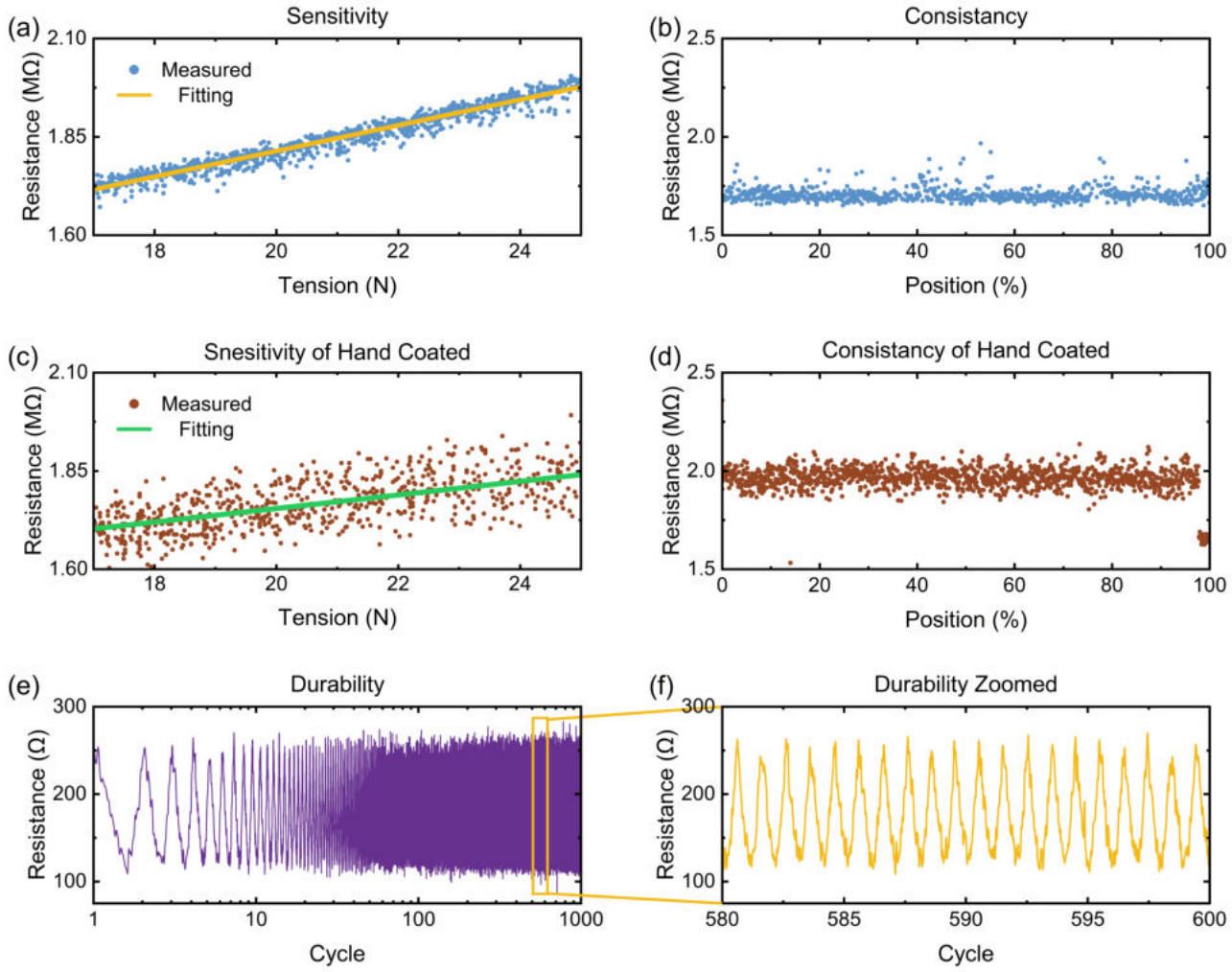

Fig. 9. (a) Measured and linear fitted sensitivity curve of the fabricated strain sensor. (b) Resistance consistency along the fabricated thread. (c) sensitivity and (d) consistency test of hand-coated thread. (e) Durability test over 1000 and (f) zoomed-in plot.

size, the moving average reduces the noise more significantly. A limitation of utilizing the moving average method is that this method introduces a delay to the system. An optimal window size can be utilized depending on the application of the thread. If the thread is stretched slowly, a larger window size can be utilized which would produce a smoother signal. For higher-frequency applications, a smaller window size would be favorable to minimize the delay and also provide desirable noise reduction. In this project, the moving average method is utilized as a sample filtering option. More advanced filtering algorithms can be utilized depending on the complexity of the application and the processing power available on the system.

IV. Applications

To demonstrate the application of the fabricated strain-sensing thread, a wearable sensor patch was designed. The sensor patch can be applied to the human body to record respiration or limb movement, depending on the placement location. Fig. 11(a) shows the block diagram of the system of the sensor patch and the measuring electronics. The strain-sensing thread is connected to a resistance trans-impedance amplifier (TIA) to characterize the resistance in real-time, followed by a 10-bit ADC and a microcontroller, which transmits the data wirelessly to a terminal. Fig. 11(b) and (c) show the sensor patch applied to the chest and elbow of a person, respectively. A piece of the strain-sensing thread was placed on a regular band-aid. Eco-flex was used to fix the thread in place with the band-aid as well as protect the thread from scratching. Conductive silver strings were used to connect the thread to the TIA. The length of the strain-sensing thread was chosen so that its initial resistance is 100 Ω.

For respiration monitoring, the band-aid was applied to the chest when the person exhaled. As the person inhales, he's chest expands, thus stretching the thread and resulting in an increase of the resistance. When the person exhales, the chest volume shrinks, allowing the thread to retract and impedance drops back to 100 Ω. Plot e in Figure 11 shows the measured respiration data in real-time. The measured

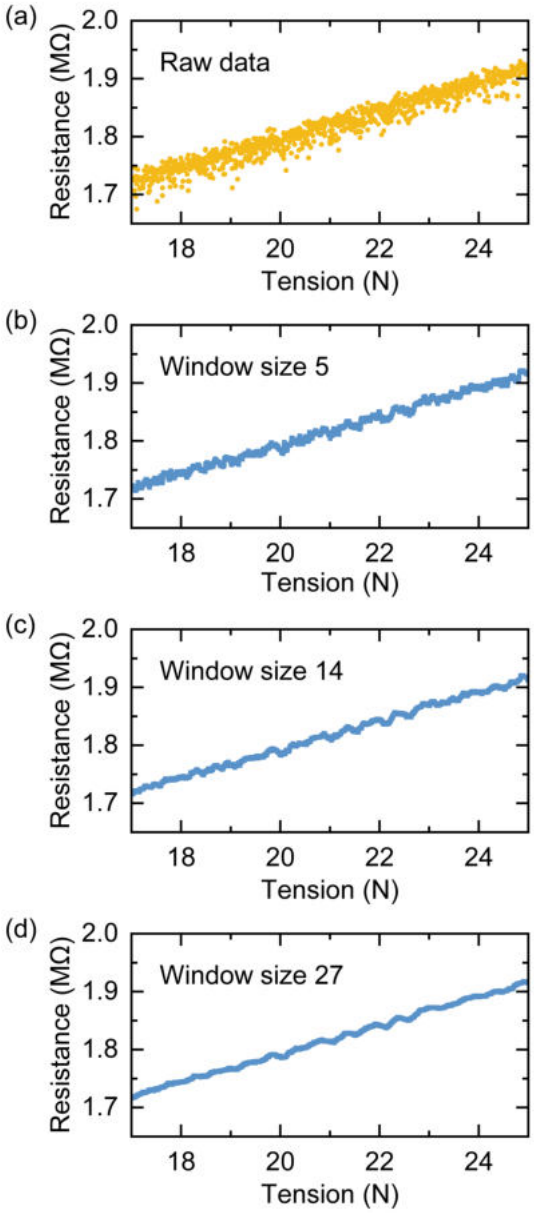

Fig. 10. (a) Raw data of sensitivity of fabricated threads, and tension-resistance relationship after applying a moving average window of (b) 5, (c) 14, and (d) 27 samples.

respiration rate is around 9 times per minute. By calibrating the initial chest circumference, one can also calculate the volume of air exchange of each breath. More complex studies such as VO_2 max can be approximated as well.

To monitor limb movement, the sensor patch was applied to the elbow. As shown in Fig. 11(c), the sensor patch stretches when the arm is bent. Fig. 11(f) shows the measured resistance for elbow flexing. At the maximum of 150° elbow flexing, the resistance of the thread increased from 100 Ω to around 550 Ω. As the elbow was relaxed, the resistance immediately decreased back to 100 Ω. When the elbow was only flexed 90°, the resistance increased to around 420 Ω. At a lower 45° flexing, the resistance only increased to 350 Ω. By mapping the resistance of the sensor patch to the elbow flexing position, one can monitor the motion of the forearm, as well as other body joints.

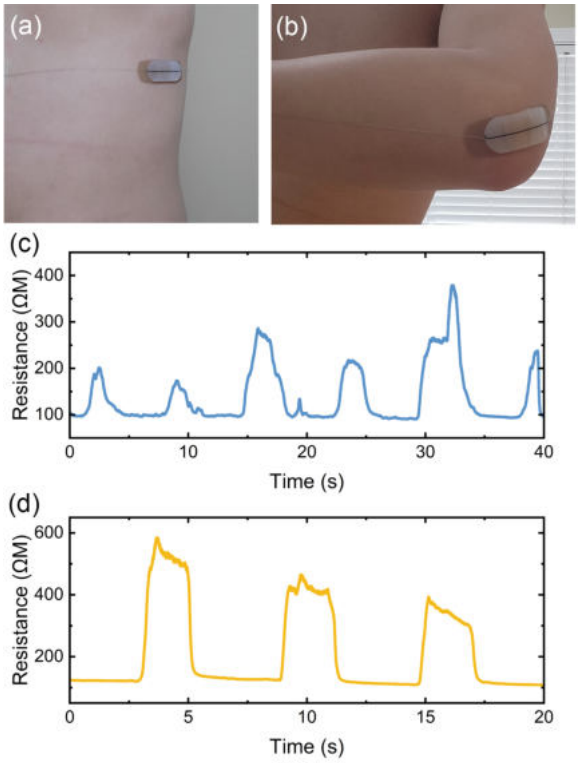

Fig. 11. Images of (a) Reparation sensing patch and (b) limb motion patch. Real-time resistance data of (c) respiration and (b) elbow motion.

V. Conclusion

In this work, an automatic strain-sensing thread-coating system was presented. The system is capable of continuously coating carbon ink onto elastic threads with controlled parameters. The fabricated thread has a linear strain-to-resistance ratio. The sensitivity is 32.64 KΩ/N, and remains unchanged after 1000 stretching cycles. Compared to the hand-coated thread, the system provides much higher consistency. To demonstrate the application of the fabricated thread, a wearable patch was designed to monitor respiration and limb motion. The strain-sensing thread converts the physical length change on the surface of the human body to resistance. Through a TIA readout and microcontroller circuit, the resistance information was wirelessly transmitted to a computer for data processing and analysis.

References

[1] Jaeyoon Park, Insang You, Sangbaie Shin, and Unyong Jeong. Material Approaches to Stretchable Strain Sensors.

[2] Jilong Wang, Chunhong Lu, and Kun Zhang. Textile-Based Strain Sensor for Human Motion Detection. *Energy Environmental Materials*, 3(1):80–100, mar 2020.

[3] Yan Wang, Li Wang, Tingting Yang, Xiao Li, Xiaobei Zang, Miao Zhu, Kunlin Wang, Dehai Wu, and Hongwei Zhu. Wearable and Highly Sensitive Graphene Strain Sensors for Human Motion Monitoring. *Advanced Functional Materials*, 24(29):4666–4670, aug 2014.

[4] Xu Liu, Yuan Wei, and Yuanying Qiu. Advanced Flexible Skin-Like Pressure and Strain Sensors for Human Health Monitoring. *Micromachines 2021, Vol. 12, Page 695*, 12(6):695, jun 2021.

[5] Hassan Khan, Amir Razmjou, Majid Ebrahimi Warkiani, Ajay Kottapalli, and Mohsen Asadnia. Sensitive and Flexible Polymeric Strain Sensor for Accurate Human Motion Monitoring. *Sensors 2018, Vol. 18, Page 418*, 18(2):418, feb 2018.

[6] Liwei Lin, Yejung Choi, Tianyu Chen, Hoonsub Kim, Kyu Sang Lee, Jeongmin Kang, Lulu Lyu, Jiefeng Gao, and Yuanzhe Piao. Superhydrophobic and wearable TPU based nanofiber strain sensor with outstanding sensitivity for high-quality body motion monitoring. *Chemical Engineering Journal*, 419:129513, sep 2021.

[7] Hongwei Zhou, Zhaoyang Jin, Ying Yuan, Gai Zhang, Weifeng Zhao, Xilang Jin, Aijie Ma, Hanbin Liu, and Weixing Chen. Self-repairing flexible strain sensors based on nanocomposite hydrogels for whole-body monitoring. *Colloids and Surfaces A: Physicochemical and Engineering Aspects*, 592:124587, may 2020.

[8] Zhiran Shen, Fanmao Liu, Shuang Huang, Hao Wang, Cheng Yang, Tian Hang, Jun Tao, Wenhao Xia, and Xi Xie. Progress of flexible strain sensors for physiological signal monitoring. *Biosensors and Bioelectronics*, 211:114298, sep 2022.

[9] Junfei Xia, Shirin Khaliliazar, Mahiar Max Hamedi, and Sameer Sonkusale. Thread-based wearable devices. *MRS Bulletin*, 46(6):502–511, jun 2021.

[10] Ping Liu, Weidong Pan, Yue Liu, Jian Liu, Wenrui Xu, Xiaohui Guo, Caixia Liu, Yugang Zhang, Yunjian Ge, and Ying Huang. Fully flexible strain sensor from core-spun elastic threads with integrated electrode and sensing cell based on conductive nanocomposite. *Composites Science and Technology*, 159:42–49, may 2018.

[11] Fei Huang, Jiyong Hu, and Xiong Yan. A wide-linear-range and low-hysteresis resistive strain sensor made of double-threaded conductive yarn for human movement detection. *Journal of Materials Science Technology*, 172:202–212, feb 2024.

[12] Hongda Ding, Yanqiu Wang, and Xiande Shen. Multifunctional Rubber Latex Threads Based on MXene@Natural Rubber/Polyacrylamide for Temperature and Strain Sensors. *ACS Applied Polymer Materials*, 5(7):4678–4688, jul 2023.

[13] Michaela Radouchova, Martin Janda, David Kalas, and Tomas Blecha. Interconnection of Highly Flexible Carbon Threads Suitable for Wearable Strain Monitoring using Ultrasonic Plastic Welding. *Proceedings of the International Spring Seminar on Electronics Technology*, 2023-May, 2023.

[14] Huixu Li, Ding Zhang, Chao Wang, Yilong Hao, Yu Zhang, Ying Li, Pingping Bao, and Heting Wu. 3D Extruded Graphene Thermoelectric Threads for Self-Powered Oral Health Monitoring. *Small*, 19(26):2300908, jun 2023.

[15] Azevedo Coste, Lucas Oliveira Da Fonseca, Jose Guillermo, Colli Alfaro, and Ana Luisa Trejos. Design and Fabrication of Embroidered Textile Strain Sensors: An Alternative to Stitch-Based Strain Sensors. *Sensors 2023, Vol. 23, Page 1503*, 23(3):1503, jan 2023.

[16] Nimal Jagadeesh Kumar, Alexander Johnson, Daniel Roggen, Niko Münzenrieder, N J Kumar, A Johnson, D Roggen, and N Münzenrieder. A Flexible Capacitance Strain Sensor with Stitched Contact Terminals. *Advanced Materials Technologies*, 8(2):2200410, jan 2023.

[17] Juyao Li, Shuang Li, Yewang Su, J Li, S Li, and Y Su. Stretchable Strain Sensors Based on Deterministic-Contact-Resistance Braided Structures with High Performance and Capability of Continuous Production. *Advanced Functional Materials*, 32(49):2208216, dec 2022.

[18] Orathai Tangsirinaruenart and George Stylios. A Novel Textile Stitch-Based Strain Sensor for Wearable End Users. *Materials 2019, Vol. 12, Page 1469*, 12(9):1469, may 2019.

[19] Zekun Liu, Yan Zheng, Lu Jin, Kaili Chen, Heng Zhai, Qiyao Huang, Zhongda Chen, Yangpeiqi Yi, Muhammad Umar, Lulu Xu, Gang Li, Qingwen Song, Pengfei Yue, Yi Li, and Zijian Zheng. Highly Breathable and Stretchable Strain Sensors with Insensitive Response to Pressure and Bending. *Advanced Functional Materials*, 31(14):2007622, apr 2021.

[20] Jean Baptiste Chossat, Yiwei Tao, Vincent Duchaine, and Yong Lae Park. Wearable soft artificial skin for hand motion detection with embedded microfluidic strain sensing. *Proceedings - IEEE International Conference on Robotics and Automation*, 2015-June(June):2568–2573, jun 2015.

[21] Mikhail A. Kanygin, Mahnaz Shafiei, and Behraad Bahreyni. Electrostatic Twisting of Core-Shell Nanofibers for Strain Sensing Applications. *ACS Applied Polymer Materials*, 2(11):4472–4480, nov 2020.

[22] Francesco Alaimo, Aydin Sadeqi, Hojatollah Rezaei Nejad, Yiwen Jiang, Wei Wang, Danilo Demarchi, and Sameer Sonkusale. Reel-to-reel fabrication of strain sensing threads and realization of smart insole. *Sensors and Actuators A: Physical*, 301:111741, jan 2020.

[23] Yiwen Jiang, Aydin Sadeqi, Eric L. Miller, and Sameer Sonkusale. Head motion classification using thread-based sensor and machine learning algorithm. *Scientific Reports 2021 11:1*, 11(1):1–11, jan 2021.

[24] Francesco Alaimo, Hojatollah Rezaei Nejad, Aydin Sadeqi, Danilo Demarchi, and Sameer Sonkusale. Wearable Flexible Touch Interface Using Smart Threads. *Proceedings of IEEE Sensors*, 2018-Octob, dec 2018.

[25] Aydin Sadeqi, Hojatollah Rezaei Nejad, Francesco Alaimo, Haiyang Yun, Meera Punjiya, and Sameer R. Sonkusale. Washable Smart Threads for Strain Sensing Fabrics. *IEEE Sensors Journal*, 18(22):9137–9144, nov 2018.